A Multi-Axis FBG-Based Tactile Sensor for Gripping in Space

Samuel Frishman[*1], Julia Di[*1], Zulekha Karachiwalla[2], Richard J. Black[3], Kian Moslehi[3], Trey Smith[4], Brian Coltin[4], Bijan Moslehi[3], Mark R. Cutkosky[1]

Abstract— Tactile sensing can improve end-effector control and grasp quality, especially for free-flying robots where target approach and alignment present particular challenges. However, many current tactile sensing technologies are not suitable for the harsh environment of space. We present a tactile sensor that measures normal and biaxial shear strains in the pads of a gripper using a single optical fiber with Bragg grating (FBG) sensors. Compared to conventional wired solutions, the encapsulated optical fibers are immune to electromagnetic interference — critical in the harsh environment of space. Sampling is possible at over 1 kHz to detect dynamic events. We mount sensor pads on a custom two-fingered gripper with independent control of the distal and proximal phalanges, allowing for grip readjustment based on sensing data. Calibrated sensor data for forces match those from a commercial multiaxial load cell with an average 96.2% RMS for all taxels. We demonstrate the gripper on tasks motivated by the Astrobee free-flying robots in the International Space Station (ISS): gripping corners, detecting misaligned grasps, and improving load sharing over the contact areas in pinch grasps.

I. INTRODUCTION

Space exploration presents vast opportunities for robotic systems as well as unique challenges. Radiation, electromagnetic interference (EMI), and extreme temperatures all limit technologies and devices used for space applications. Nevertheless, robots and automation are central to enabling exploration of distant and dangerous locations. The importance of tactile sensing in robotic systems designed for unstructured and unknown environments is increasingly recognized [1], [2]. Prevalent sensing technologies, including capacitive, piezoresistive, and optical transducers based on imaging, are susceptible to electromagnetic interference and often require processing circuitry physically near the sensor. In this work, we introduce a multiaxial optical tactile sensor for robotic grippers in space (Fig. 1). The initial version is designed for the Astrobee free-flyer platform inside the ISS [3], as a first step toward extravehicular applications.

Among the many technologies considered for tactile sensing, optical fiber sensors provide a number of advantages including EMI immunity, tolerance of vibration and impact, resistance to corrosion, and resistance to extreme temperatures (cryogenic to $1000°$C) and radiation [4]–[6]. Moreover,

FBGs exhibit excellent signal-to-noise ratio (SNR) and sensitivity to very small strains. They can also route over long distances with negligible loss.

We introduce a novel tactile sensor using a single optical fiber routed through four sensing structures embedded in an elastomeric pad. The sensor pads are mounted on a two-finger two-phalange gripper. In the following sections we describe the sensor and gripper designs and report on experiments conducted to characterize the sensor and demonstrate its performance. Calibration experiments show that the pads match force data from a commercial load cell with 96.2% RMS accuracy. We present demonstrations of using tactile data to modulate the grasp force and make adjustments to improve contact and load sharing when grasping large and small objects with initial misalignment. In future work, we discuss extensions to extra-vehicular applications that will require the durability afforded by optical fibers.
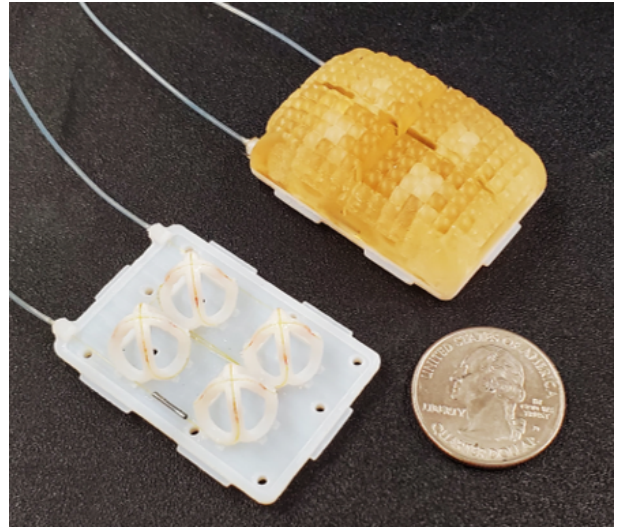

Fig. 1. An FBG-based, multi-axis sensing pad. Tower structures, each housing four FBGs, provide three-axis force information at each structure. An additional FBG is isolated and adhered inside a metal sleeve for temperature compensation. The sensing unit is encapsulated in a urethane elastomer, which serves as the gripping surface. Deep grooves in the pad decouple the signals between towers.

A. Related Work

FBGs provide strain information through changes in detected wavelength. Their durability is leveraged in a wide range of applications including oil and gas [7], wind energy [8], and medical devices [9], but to date, FBG-based tactile sensors have been largely limited to single-axis sensing (e.g.

---

[*]These authors contributed equally

[1] Stanford University, Department of Mechanical Engineering, Stanford, California 94305

[2] University of Maryland, Department of Computer Engineering, Baltimore, Maryland 21250

[3] Intelligent Fiber Optic Systems Corporation, San Jose, California 95134

[4] NASA Ames, Mountain View, California 94035

pressure or grip force) [10]–[16]. Meanwhile, embodiments capable of multi-axis sensing are comparatively large (e.g. designed for use as a multi-axis force/torque sensor) [17], [18] or embedded directly into gripper fingers [19]–[21]. Opportunities remain to use FBG technology for sensing spatially-distributed, multi-axis forces on gripper phalanges. Understanding the grasp contact area and phalange-object alignment can improve grasp quality (e.g. of a hand rail or tool). The importance of these parameters has been noted in particular for underactuated grippers [22], [23]. Typically, underactuated end-effector designs involve a trade-off between the ratios of joint torques and stiffnesses to achieve desired hand closure patterns as well as grasp stability. For example, Ciocarlie et al. [24] tune spring stiffnesses to maintain a parallel constraint on the distal phalanges, unless contact is made proximally, enabling planar contact in pinch grasps. Linkage mechanisms have also been explored to achieve similar capabilities [25], [26]. For free-flying robots such as Astrobee, misalignment on initial contact may be common. We therefore control two degrees of freedom to enable grasp readjustment based on multiaxial tactile data.

II. Sensor Design

We present a tactile sensing pad composed of four isolated sensing towers, each with four FBGs, totaling 16 strain-sensing FBGs. An additional strain-isolated FBG provides temperature compensation so that the entire sensor consists of 17 FBGs, all routed along a single fiber.

In contrast to designs that utilize bending loss, FBG-based sensors are discrete measurements of fiber axial strain with high accuracy—essentially, individual optical strain gauges. The FBGs are read using an interrogator, which detects the shifts in wavelength of reflected light caused by an external strain. FBGs each have a unique characteristic wavelength and can be read simultaneously. More discussion on the principles of FBGs as strain sensors can be found in [27].

Sensor design is constrained by optical fiber requirements where fiber routing must satisfy a set minimum bend radius and accommodate pre-determined FBG lengths. For $125\,\mu$m and $80\,\mu$m fibers, bend radii should not fall below $6\,$mm and $4\,$mm, respectively; typical FBG lengths are either $4\,$mm or $2\,$mm. These dimensions govern the sensing pad design required to fit within a small gripper while providing multiaxial sensing. The resulting tower structure is illustrated in Fig 2. The fiber routes through grooves in the four curved pillars that make up each tower. The depth of the groove on each pillar is just sufficient to align the fiber and hold it with cyanoacrylate adhesive. The pillars are $4\,$mm in length, accommodating a $2\,$mm FBG with a $1\,$mm buffer on either end. It is critical for FBGs to be placed on a straight section of the pillar to avoid double peaks in signal [10]. Pillar angle, θ_p, determines structure sensitivity to normal vs. shear forces. For this prototype, informed by FEA analysis as described below, a $70°$ angle is selected to achieve a desirable balance between normal and shear sensitivity. These parameters define the tower geometry.

Because of the large number of relatively tight bends, the routed fiber has some signal attenuation down its length. Therefore, we read the fiber from both ends, using the stronger of the corresponding FBG signals for data (Fig. 2B).

The structure is printed on the Stratasys Objet24 (VeroWhitePlus) and cast inside a urethane elastomer (Smooth-On VytaFlex 20). The urethane cover includes deep grooves separating each tower for signal decoupling across towers. To fit on a gripper phalange, each sensor is slightly longer than it is wide. Fig. 2C presents sample strain data gathered from all four towers with only one tower under loading. Large microstrain values are observed by the tower under loading (FBGs 1-4), with minimal signal from adjacent towers ("Others").
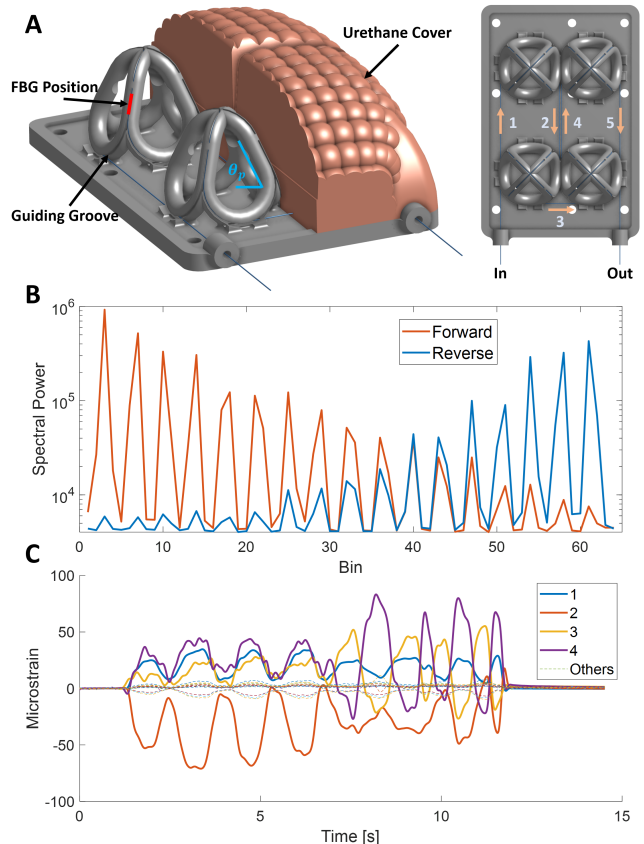

Fig. 2. (A) The sensing structures and urethane pad are shown. Structures include grooves to guide the fiber and features to fix the FBG along the straight sections of each pillar (red). (B) The single fiber is read from both forward and reverse directions to minimize attenuation. Seventeen peaks are visible, corresponding to each FBG; the strongest signal for a given FBG is used. (C) Sample data gathered while applying loads on a single taxel: colored lines 1-4 show signals from FBGs in the loaded tower; other FBGs (dashed lines) from the other towers provide little signal.

A. Finite element model

We used a preliminary finite element analysis (FEA) to inform the sensor design, investigating the placement of cutout features to increase strains locally at the FBGs and the placement of the FBGs relative to the neutral axes of the tower legs. The cutouts promote bending in the pillars,

FBG Location

Cutout

ESTRN

2.000e-04
1.800e-04
1.600e-04
1.400e-04
1.200e-04
1.000e-04
8.000e-05
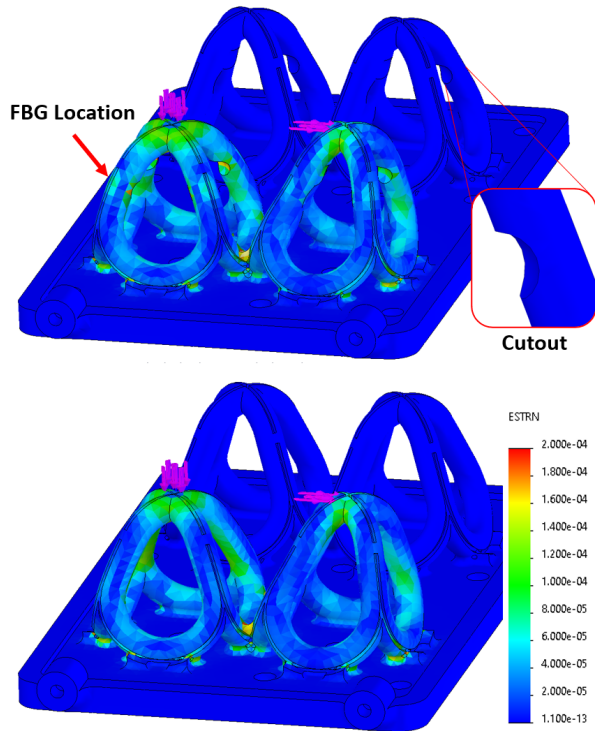6.000e-05
4.000e-05
2.000e-05
1.100e-13

Fig. 3. Finite element analysis (structure deformation is exaggerated). Normal and shear forces are applied to the tower structures. (Top) The structure includes cutout features in the pillars. (Bottom) The structure is shown without cutout features. Significantly more strain is observed at the FBGs locations when cutouts are present. Tower angle results in a desirable ratio between normal and shear force sensitivity.

which are otherwise substantially affected by axial strain. In a weightless environment, and specifically for Astrobee tasks, shear forces are expected to be relatively small compared to normal loads. Accordingly, pillar angle is tuned for increased shear sensitivity. In the FEA, we apply a 1 N normal force and 0.33 N shear with results shown in Fig. 3. The initial FEA is approximate but sufficiently accurate for small forces to inform FBG placement. Future FEA analysis will be conducted as we move from the current prototyping materials to sintered ceramic towers and space-qualified polymers.

III. GRIPPER DESIGN

The sensor pads are mounted on a custom, two-finger two-phalange gripper (Fig. 4) intended for use with the Astrobee free flyer [3]. The gripper is underactuated, but provides independent control of the distal and proximal phalanges. The distal phalange has the ability to hyperextend to achieve planar contact for pinch or corner grasps. Two motors are located inside the gripper body and provide tendon tension to the proximal and distal phalanges, respectively. Torsion springs in each joint provide extension. The design also includes a "distal backboard" that is engaged during distal hyperextension. The backboard is preloaded with a spring and pushes against the distal phalange, forcing the phalange inward when engaged. A hard stop prevents the backboard from engaging when the phalange is flexed inward beyond the midpoint of its range of motion. This provision makes

the distal joint stiffer when hyperextended and extends the overall grasp envelope, while also allowing planar contact in pinch grasps as the fingers close together. The motor actuating the proximal phalange must overpower the backboard for hyperextension to occur; therefore the backboard spring is preloaded to only slightly increase the torque required of the distal torsion spring.

The gripper body houses two Portescap gearmotors (16G 214E, 27:1), one for each of the two tendons that actuate both of the proximal and distal phalanges, respectively. Figure 4 illustrates routing paths in the proximal and distal phalanges (only one side of each tendon routing is shown for simplicity). The motors and pulleys are sized to provide 70 N of tension in the cables, achieving a ≈ 4 N grasp force in pinch. Moreover, the selected gearmotors are backdrivable, which is useful for compliant grasp adjustment. Tendons are anchored to swivel-head screws for tensioning. Hard stop features at the proximal and distal joints limit extension and allow preloading of the joint torsion springs.

Sensor

Anchor

Backboard

Proximal
Distal
Backboard

Backboard Spring

Stopper

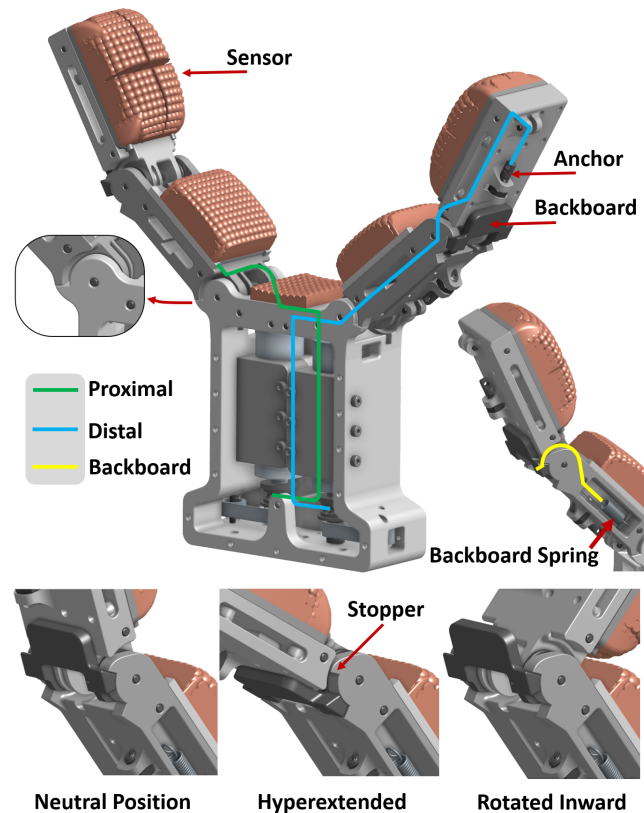Neutral Position   Hyperextended   Rotated Inward

Fig. 4. The two-finger gripper has sensing pads mounted at the distal phalanges. Two motors route to independent proximal and distal tendons, providing an underactuated design with two controllable DoF (only one side of each tendon routing shown for simplicity). A backboard feature, loaded by a spring embedded inside the proximal phalange, provides a biasing inward force on the distal joint when extended beyond the neutral position. The backboard stiffens the distal phalange during hyperextension.
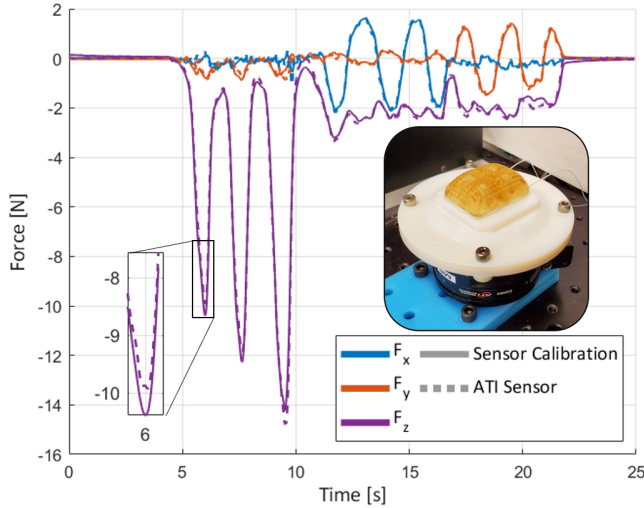
Fig. 5. Sensor calibration of normal and shear forces compared to the ATI force/torque sensor, with R^2 = 0.99. Inset at left shows an enlarged view of the first trough to highlight the small differences in FBG and ATI signals. Forces are applied manually to each taxel and transmitted through the substrate to the ATI sensor beneath, as shown inset at right.

IV. EXPERIMENTS

A. Calibration

We calibrate the sensor by mounting the pad on a commercial ATI Gamma force/torque load cell and manually applying forces with a flat, rigid object. Each sensor taxel is calibrated independently. The test setup is shown in the inset of Fig. 5.

The acquisition frequency can be up to 6 kHz, but for the purposes of calibration we sample the FBGs and load cell at 100 Hz and apply low pass filters with a cutoff frequency of 15 Hz. For each taxel, a second-order polynomial is fit to the corresponding (x, y, z) forces from the load cell. We use a polynomial calibration because some nonlinearity is expected, given that the sensor consists of polymeric materials cast in an elastomer. Although the sensor response is not linear, the nonlinearity is characterizable after a few calibration grasps before use. For the taxel calibration shown in Fig. 5, we achieve an R^2 value of 99.6% on our training data, with a cross-validation R^2 of 97.3% on unseen data, indicating a close fit to the ATI. For all taxels from both sensors, we obtain calibration R^2 values above 90%, with an average value of 96.2% across taxels. Coupling between pillars may contribute to calibration error, though we note that the structure produces distinct signal patterns for different loading conditions. Moreover, information from multiple towers can resolve potential redundant configurations arising from torque and shear loading. We observed little hysteresis during calibration testing, with more rigorous hysteresis analysis to be done in the future with a sensor made from space-ready materials.

B. Grasping Evaluation

Figure 6 shows several grasps motivated by expected manipulation tasks such as fetching boxes or tools with the Astrobee free flyer. Three conditions are explored: (1) detection of misalignment with an object, which is especially a concern for free-flying robots; (2) perception of shear forces during object pullout, and (3) grasp adjustment to achieve planar contact for increased grasp stability.

1) Detection of Misalignment: In this task, the gripper is rotated to $\approx 20°$ and closed on a vertical object (see Fig. 7A for geometry). The object makes contact with the distal phalange at an angle. The misalignment can be deduced based on which taxels loaded and the resulting force vector.

2) Shear Force Perception: In the second task, a pinch grasp is performed on a thin acrylic sheet (Fig. 7B). The acrylic is pulled away from the gripper with varying force and sensor data are recorded.

3) Grasp Adjustment: Independent control of the proximal and distal phalanges enables grasp adjustment to increase the contact area. Specifically, achieving planar contact at the distal phalanges during pinch or corner grasps of flat objects significantly improves grasp stability [28]. In this experiment, we demonstrate such capability using tactile information. The distal phalange "rolls" onto the surfaces, contacting the front taxels first and then the rear as the phalange hyperextends. Planar contact is determined when the normal forces at the front and rear taxels are approximately equal.

V. RESULTS

Typical results of the three grasping experiments are shown in Fig. 7.

Detection of Misalignment: In sub-figure A, the plots illustrate the sensor's ability to detect a misaligned grasp. The object is initially misaligned, resulting in a multi-component force vector. When aligned, the force is primarily normal to the sensor surface in the F_z direction. Contact force orientation can also be deduced from the directional loads sensed on each taxel.

Perception of Shear: Sub-figure B depicts the sensor's ability to perceive shear forces as an object is pulled from its grasp. As the object is pulled, an increase in normal force (F_z) is also observed due to mechanical coupling in the underactuated gripper; the rear taxels roll into the object as the object is pulled. The plot presents data for a rear taxel, illustrating the expected effect.

Grasp Adjustment: Sub-figure C presents data from two taxels of a single sensor, one in the front and one in the rear. Contact events are annotated. The front taxel makes initial contact as the finger rotates. The phalange rolls further onto the surface, with loading on the rear taxel visible. The normal force distribution between the taxels is then adjusted until planar contact is reached.

VI. DISCUSSION

The presented sensor and gripper combination provides the ability to perform a wide range of anticipated grasps with the Astrobee free flyer while simultaneously perceiving contact conditions. Preliminary tests demonstrate detection of grasp misalignment, shear forces, and grasp readjustment. We largely focus on achieving planar contact at the distal
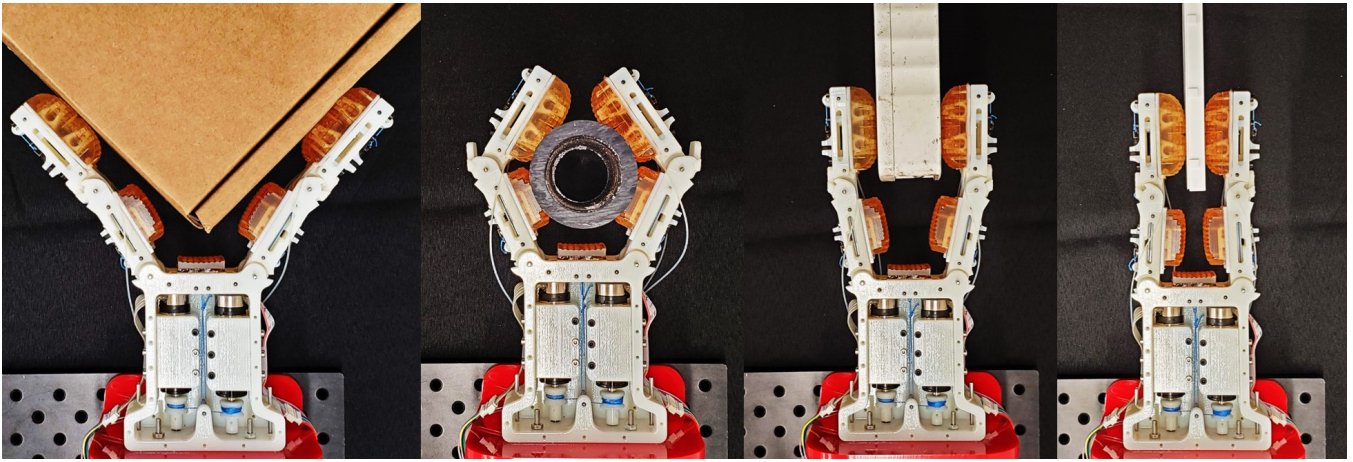
Fig. 6. Demonstrations of several grasps using sensor data to monitor grasp conditions. (From left) A corner grasp with planar contact, demonstrating distal hyperextension; an enveloping grasp around a polycarbonate tube; a pinch grasp on rectangular plastic box; a pinch grip on thin plastic plate.
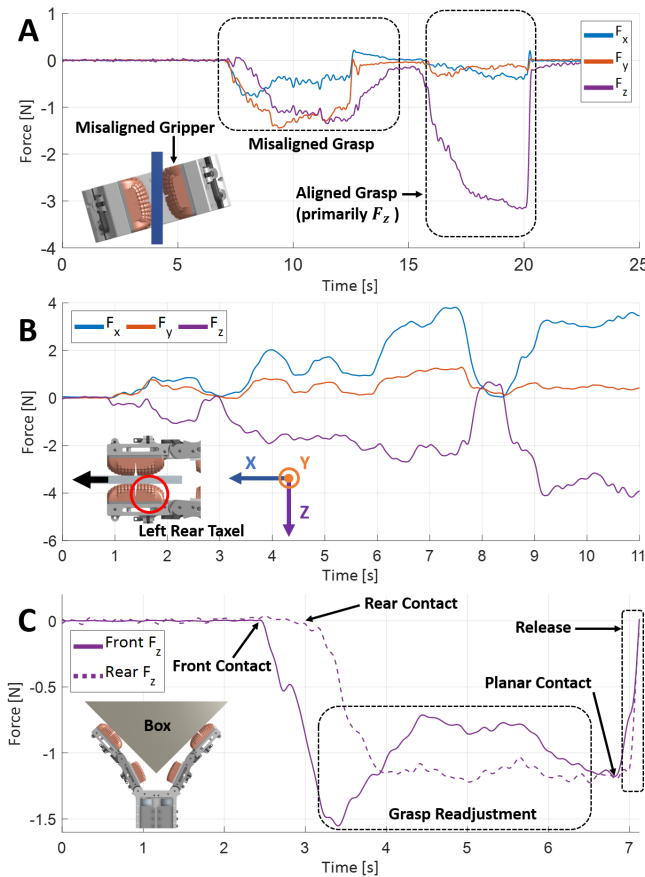

Fig. 7. Three grasp experiments. (A) *Grasp Misalignment:* the gripper is first rotated to a misalignment angle and closed on a vertical object. Then an aligned grasp is attempted. The data shown are for the left finger, for which the left rear taxel makes contact. (B) *Shear Force:* the gripper holds an acrylic plate which is tugged several times in the x direction with increasing intensity. Shear and normal forces for the left rear taxel are plotted. Mechanical coupling in the gripper causes the z force to vary along with the x force; the y force is largely unaffected. (C) *Planar Contact:* The gripper performs a corner grasp on a box. Spatial distribution of the sensing towers enables perception of grasp events and planar contact.

phalange to improve grasp stability in corner and pinch grasps. For corner grasps specifically, such an approach reduces the chances of object ejection (slipping out of the grasp as the fingers close)—particularly a concern for free-flying robots and objects.

Figure 7B illustrates the gripper's ability to detect shear forces. Such functionality provides benefit when manipulating tools and moving objects. Moreover, understanding multi-axis forces is conducive to collaborative tasks between the Astrobee and astronauts or between multiple free-flyers. Astrobee groups can transport and manipulate large objects, monitoring load sharing via the tactile sensors.

VII. CONCLUSIONS AND FUTURE WORK

We have presented a multi-axis tactile sensor and an associated gripper for the Astrobee free-flyer. The sensor employs a single optical fiber with 17 FBGs spaced across multiple sensing towers, enabling a compact design. We report on early grasp experiments and demonstrate the sensors' ability to provide gripper alignment information, detect shear forces, and enable grasp readjustments.

In the near term, experiments will be conducted with the gripper mounted on a planar free-floating platform [29] to investigate the ability to perform corner grasps, potentially with initial misalignment, in more detail. Of particular interest is controlling the hand and platform to minimize the chance of ejecting objects from the grasp.

In these next experiments, adding a sensing pad to the proximal phalanges may increase functionality, particularly for enveloping grasps. With increased sensing, slip detection, surface texture identification, and other dynamic phenomena are also of interest, taking advantage of the ability to sample the FBGs at over 1 kHz. Subsequent sensor designs will use additional FEA to examine the polymer cover and include non-linear capabilities.

Preliminary tests also suggest a change to the motor/transmission ratios. In the current prototype, identical motors are used for the proximal and distal phalanges for simplicity. However, the roles of the motors are different: in

addition to experiencing a larger torque from grasp forces, the proximal motor must extend the backboard spring to achieve distal hyperextension. Moreover, it must have sufficient torque to overcome the effect of the distal motor when holding a given position. In future prototypes, a larger gear ratio will be used for the proximal tendon. We note that backdrivability is less critical in the proximal phalange, though some compliance is desirable for safety.

While the initial prototype sensor and gripper are designed for the Astrobee inside the ISS, our technology vision includes extravehicular applications (EVA). We have explored ceramic structures, rather than the plastic towers presented here, using 3D printed ceramics (Formlabs Form2 printer). A ceramic structure provides a much wider operating temperature range and exhibits a coefficient of thermal expansion closer to the glass fiber, reducing challenges with thermal strain and bonding to the pillars. For EVA use, the urethane pads could be replaced by a low-outgassing space-qualified silicone RTV compound [30].

ACKNOWLEDGMENT

REFERENCES

[1] M. R. Cutkosky and W. Provancher, "Force and tactile sensing," in *Springer Handbook of Robotics*. Springer, 2016, pp. 717–736.

[2] A. Yamaguchi and C. G. Atkeson, "Recent progress in tactile sensing and sensors for robotic manipulation: can we turn tactile sensing into vision?" *Advanced Robotics*, vol. 33, no. 14, pp. 661–673, 2019.

[3] I.-W. Park, T. Smith, H. Sanchez, S. W. Wong, P. Piacenza, and M. Ciocarlie, "Developing a 3-dof compliant perching arm for a free-flying robot on the international space station," in *2017 IEEE International Conference on Advanced Intelligent Mechatronics (AIM)*. IEEE, 2017, pp. 1135–1141.

[4] U. Sampath, D. Kim, H. Kim, and M. Song, "Polymer-coated fbg sensor for simultaneous temperature and strain monitoring in composite materials under cryogenic conditions," *Applied optics*, vol. 57, no. 3, pp. 492–497, 2018.

[5] F. Huang, T. Chen, J. Si, X. Pham, and X. Hou, "Fiber laser based on a fiber bragg grating and its application in high-temperature sensing," *Optics Communications*, vol. 452, pp. 233–237, 2019.

[6] G. Berruti, M. Consales, M. Giordano, L. Sansone, P. Petagna, S. Buontempo, G. Breglio, and A. Cusano, "Radiation hard humidity sensors for high energy physics applications using polyimide-coated fiber bragg gratings sensors," *Sensors and Actuators B: Chemical*, vol. 177, pp. 94–102, 2013.

[7] X. Qiao, Z. Shao, W. Bao, and Q. Rong, "Fiber bragg grating sensors for the oil industry," *Sensors*, vol. 17, no. 3, p. 429, 2017.

[8] S. Park, T. Park, and K. Han, "Real-time monitoring of composite wind turbine blades using fiber bragg grating sensors," *Advanced Composite Materials*, vol. 20, no. 1, pp. 39–51, 2011.

[9] D. L. Presti, C. Massaroni, C. S. J. Leitão, M. D. F. Domingues, M. Sypabekova, D. Barrera, I. Floris, L. Massari, C. M. Oddo, S. Sales, *et al.*, "Fiber bragg gratings for medical applications and future challenges: A review," *IEEE Access*, vol. 8, pp. 156 863–156 888, 2020.

[10] J.-S. Heo, J.-H. Chung, and J.-J. Lee, "Tactile sensor arrays using fiber bragg grating sensors," *Sensors and Actuators A: Physical*, vol. 126, no. 2, pp. 312–327, 2006.

[11] J.-S. Heo, J.-Y. Kim, and J.-J. Lee, "Tactile sensors using the distributed optical fiber sensors," in *2008 3rd International Conference on Sensing Technology*. IEEE, 2008, pp. 486–490.

[12] J. Song, Q. Jiang, Y. Huang, Y. Li, Y. Jia, X. Rong, R. Song, and H. Liu, "Research on pressure tactile sensing technology based on fiber bragg grating array," *Photonic Sensors*, vol. 5, no. 3, pp. 263–272, 2015.

[13] T. Li, C. Shi, and H. Ren, "A high-sensitivity tactile sensor array based on fiber bragg grating sensing for tissue palpation in minimally invasive surgery," *IEEE/ASME Transactions on Mechatronics*, vol. 23, no. 5, pp. 2306–2315, 2018.

[14] Q. Jiang and L. Xiang, "Design and experimental research on small-structures of tactile sensor array unit based on fiber bragg grating," *IEEE Sensors Journal*, vol. 17, no. 7, pp. 2048–2054, 2017.

[15] S. Samuel, A. Kumar, and C. K. Mukhopadhyay, "Fiber bragg grating tactile sensor for imaging," *Optik*, vol. 198, p. 163062, 2019.

[16] L. Massari, E. Schena, C. Massaroni, P. Saccomandi, A. Menciassi, E. Sinibaldi, and C. M. Oddo, "A machine-learning-based approach to solve both contact location and force in soft material tactile sensors," *Soft robotics*, vol. 7, no. 4, pp. 409–420, 2020.

[17] S. Hu, H. Wang, Y. Wang, and Z. Liu, "Design of a novel six-axis wrist force sensor," *Sensors*, vol. 18, no. 9, p. 3120, 2018.

[18] L. Xiong, Y. Guo, G. Jiang, X. Zhou, L. Jiang, and H. Liu, "Six-dimensional force/torque sensor based on fiber bragg gratings with low coupling," *IEEE Transactions on Industrial Electronics*, 2020.

[19] Y.-L. Park, S. C. Ryu, R. J. Black, K. K. Chau, B. Moslehi, and M. R. Cutkosky, "Exoskeletal force-sensing end-effectors with embedded optical fiber-bragg-grating sensors," *IEEE Transactions on Robotics*, vol. 25, no. 6, pp. 1319–1331, 2009.

[20] L. Massari, C. M. Oddo, E. Sinibaldi, R. Detry, J. Bowkett, and K. C. Carpenter, "Tactile sensing and control of robotic manipulator integrating fiber bragg grating strain-sensor," *Frontiers in neurorobotics*, vol. 13, p. 8, 2019.

[21] L. Jiang, K. Low, J. Costa, R. J. Black, and Y.-L. Park, "Fiber optically sensorized multi-fingered robotic hand," in *2015 IEEE/RSJ International Conference on Intelligent Robots and Systems (IROS)*. IEEE, 2015, pp. 1763–1768.

[22] R. R. Ma and A. M. Dollar, "Linkage-based analysis and optimization of an underactuated planar manipulator for in-hand manipulation," *Journal of Mechanisms and Robotics*, vol. 6, no. 1, 2014.

[23] L. U. Odhner, L. P. Jentoft, M. R. Claffee, N. Corson, Y. Tenzer, R. R. Ma, M. Buehler, R. Kohout, R. D. Howe, and A. M. Dollar, "A compliant, underactuated hand for robust manipulation," *The International Journal of Robotics Research*, vol. 33, no. 5, pp. 736–752, 2014.

[24] M. Ciocarlie, F. M. Hicks, R. Holmberg, J. Hawke, M. Schlicht, J. Gee, S. Stanford, and R. Bahadur, "The velo gripper: A versatile single-actuator design for enveloping, parallel and fingertip grasps," *The International Journal of Robotics Research*, vol. 33, no. 5, pp. 753–767, 2014.

[25] Y. Tlegenov, K. Telegenov, and A. Shintemirov, "An open-source 3d printed underactuated robotic gripper," in *2014 IEEE/ASME 10th International Conference on Mechatronic and Embedded Systems and Applications (MESA)*. IEEE, 2014, pp. 1–6.

[26] L.-A. A. Demers, S. Lefrançois, and J.-p. Jobin, "Gripper having a two degree of freedom underactuated mechanical finger for encompassing and pinch grasping," Mar. 10 2015, uS Patent 8,973,958.

[27] C. E. Campanella, A. Cuccovillo, C. Campanella, A. Yurt, and V. M. N. Passaro, "Fibre bragg grating based strain sensors: Review of technology and applications," *Sensors*, vol. 18, no. 9, 2018.

[28] G. A. Kragten and J. L. Herder, "The ability of underactuated hands to grasp and hold objects," *Mechanism and Machine Theory*, vol. 45, no. 3, pp. 408–425, 2010.

[29] M. Mote, M. Egerstedt, E. Feron, A. Bylard, and M. Pavone, "Collision-inclusive trajectory optimization for free-flying spacecraft," *Journal of Guidance, Control, and Dynamics*, vol. 43, no. 7, pp. 1247–1258, 2020.

[30] A. Parness, M. Heverly, E. Hilgemann, D. Copel, N. Wettels, T. Hilgendorf, V. White, and B. Kennedy, "On-off adhesive grippers for earth-orbit," in *AIAA SPACE 2013 Conference and Exposition*, 2013, p. 5533.